Interleaved LLC Resonant Converter With Hybrid Rectifier and Variable-Frequency Plus Phase-Shift Control for Wide Output Voltage Range Applications

Hongfei Wu, *Member, IEEE*, Xiaohai Zhan, and Yan Xing, *Member, IEEE*

***Abstract*—A family of two-phase interleaved *LLC* (iLLC) resonant converter with hybrid rectifier is proposed for wide output voltage range applications. The primary sides of the two *LLC* converters are in parallel, and the connection of the secondary windings in the two *LLC* converters can be regulated by the hybrid rectifier according to the output voltage. Variable frequency control is employed to regulate the output voltage and the secondary windings are in series when the output voltage is high. Fixed-frequency phase-shift control is adopted to regulate the configuration of the secondary windings as well as the output voltage when the output voltage is low. The output voltage range is extended by adaptively changing the configuration of the hybrid rectifier, which results in reduced switching frequency range, circulating current, and conduction losses of the *LLC* resonant tank. Zero voltage switching and zero current switching are achieved for all the active switches and diodes, respectively, within the entire operation range. The operation principles are analyzed and a 3.5 kW prototype with 400 V input voltage and 150–500 V output voltage is built and tested to evaluate the feasibility of the proposed method.**

***Index Terms*—*LLC* resonant converter, phase-shift control, rectifier, variable configuration, wide voltage range.**

I. Introduction

LLC resonant converter is one of the most attractive topologies for its features of excellent soft-switching performance and high-power density. It has been applied in several applications such as server farms [1], LED drivers [2], battery chargers [3], electric vehicles [4], renewable power systems [5], etc. Although extensive researches on design, modeling, and control of *LLC* resonant converters have been carried out by academia and industry departments, *LLC* resonant converters are still evolving [6], [7]. Tradeoff between conversion efficiency and operation range is still necessary to meet the needs of various applications. As a result, new topological variations and innovations have been continuously emerging.

Manuscript received May 30, 2016; revised July 12, 2016; accepted August 18, 2016. Date of publication August 24, 2016; date of current version February 11, 2017. This work was supported in part by the National Natural Science Foundation of China under Grant 51677085 and Grant 51407092, and in part by the Natural Science Foundation of Jiangsu Province, China under Grant BK20140812 and Qing Lan Project. Recommended for publication by Associate Editor Dr. M. Ponce-Silva. (*Corresponding author: Hongfei Wu*).

The authors are with the Center for More-Electric-Aircraft Power System, College of Automation Engineering, Nanjing University of Aeronautics and Astronautics, Nanjing 211106, China (e-mail: wuhongfei@nuaa.edu.cn; zhanxiaohai@nuaa.edu.cn; xingyan@nuaa.edu.cn).

Color versions of one or more of the figures in this paper are available online at http://ieeexplore.ieee.org.

Digital Object Identifier 10.1109/TPEL.2016.2602545

It has been recognized that soft-switching performance, high-power density and high efficiency are the most attractive features of *LLC* resonant converters. It also came to recognize that *LLC* resonant converters have some drawbacks. For example, zero current switching (ZCS) will be lost for the rectifying diodes if the switching frequency f_s is higher than the resonant frequency f_r of the resonant tank. In addition to the loss of ZCS, it is difficult to regulate the output voltage of a *LLC* resonant converter in the $f_s > f_r$ region because the voltage-gain curve in the $f_s > f_r$ region is very flat, especially in light load condition. Therefore, *LLC* resonant converters are always designed to operate in the $f_s \leq f_r$ region, where zero voltage switching (ZVS), ZCS, and good regulation of output voltage can be achieved easily [8]. However, it is still very difficult to realize a wide range of voltage/load regulation while maintaining high efficiency within the entire voltage and load ranges when $f_s \leq f_r$ [9]. It is because the increased circulating current of the resonant tank will hurt the conversion efficiency greatly once the operating frequency is far away from the resonant frequency. As a result, how to achieve high efficiency in a wide voltage range by a *LLC* resonant converter has been an emergent research topic, especially for the applications of renewable energy and battery chargers for electric vehicles.

To improve the *LLC* resonant converter's operational voltage range as well as conversion efficiency within the entire operation range, quite a few methods have been proposed. Optimal design methods were proposed to extend the operational voltage range and make full use of the voltage regulation and power conversion capabilities of *LLC* resonant converters [10]–[12]. However, the contradiction between efficiency and voltage range is still inevitable. Burst mode control is employed to improve the conversion efficiency at low output voltage and light load conditions [13]–[15]. It is straightforward and effective, but the implementation is complicated. Meanwhile, low-frequency current and voltage ripples will be introduced by the burst mode operation. Primary-side and secondary-side phase-shift control were proposed to provide another effective control freedom, so as to reduce the switching frequency range of the *LLC* resonant converter [16], [17]. Although the conduction losses associated with the circulating current of the magnetizing inductance are reduced, the turn-off losses of switches are increased because of the high turn-off current. Another straightforward and effective method to solve the wide voltage range problem is to use variable-structure topologies. Quite a few methods

have been proposed to change the circuit topology of a *LLC* resonant converter according to the input and output voltages. Variable structure *LLC* resonant converter can be achieved by changing the topology of the primary-side switching network [18], regulating the equivalent turns ratio of the transformer [19], and varying the circuit of the secondary-side rectifier [20]. However, the primary-side variable-structure topologies proposed in [18] and [19] are unsuitable for the wide output voltage range with constant input voltage applications, e.g., the battery charger for electric vehicles. It is because the core and conduction losses associated with the flux and the magnetizing current of the transformer increase when the output voltage increases. The secondary-side variable-structure rectifier proposed in [20] is a good candidate for wide output voltage range *LLC* resonant converter, but this rectifier is only valid for voltage doubler rectifier and cannot be extended to other types of rectifier. Meanwhile, two active switches have to be used on the secondary side, results in complicated control and driving of the circuit. Another secondary-side variable-structure topology is proposed for pulse width modulation (PWM) full-bridge converter by changing the connection of multiple rectifiers [21], but this method is not valid for resonant converter because smooth mode transition is very difficult to achieve and additional conduction losses will be introduced by the auxiliary switch and diode on the secondary side. In [22]–[25], novel voltage regulation method with transformer winding series-parallel auto-regulated principles is proposed for PWM forward and full-bridge converters. This method is a good candidate for PWM converters with wide output voltage range applications. However, the conversion efficiency of these PWM converters is still slight lower than resonant converters, because the rectifying diodes are hard-switched and have to sustain a high-voltage stress induced by the leakage inductance of the transformer.

The major contribution of this paper is to propose a novel voltage regulation method for *LLC* resonant converters through innovative hybrid rectifier and control method. A family of novel interleaved *LLC* (iLLC) resonant converters is harvested for wide output voltage applications. With the proposed topologies and control, the *LLC* resonant converters always operate in the $f_s \leq f_r$ region and the switching frequency range can be narrowed significantly. This paper is organized as follows. In Section II, the basic idea used to derive iLLC resonant converters with hybrid rectifier is proposed. Operation principles of a full-bridge iLLC resonant converter with hybrid full-bridge rectifier are analyzed in Section III. Characteristics of the proposed iLLC resonant converter are presented in Section IV. Experimental results are presented in Section IV. Finally, conclusions will be given in Section VI.

II. Proposed iLLC Resonant Converter With Hybrid Rectifier

The structure of the proposed iLLC resonant converter with a hybrid rectifier is shown in Fig. 1, where two *LLC* resonant switching networks are employed on the primary side and a hybrid rectifier is adopted on the secondary side. The two *LLC* resonant switching networks are connected in parallel, while the hybrid rectifier on the secondary side is shared by the two

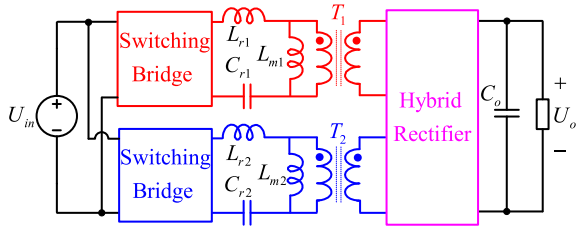

Fig. 1. Structure of the proposed iLLC resonant converter with a hybrid rectifier.

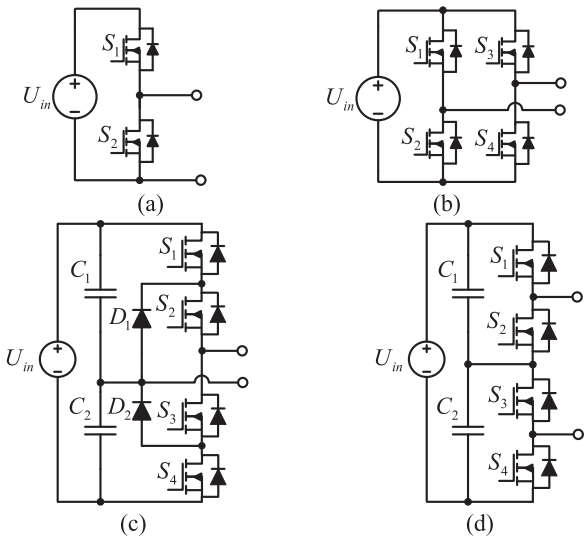

Fig. 2. Topology of the primary-side switching bridge, (a) half-bridge, (b) full-bridge, (c) and (d) three-level bridge.

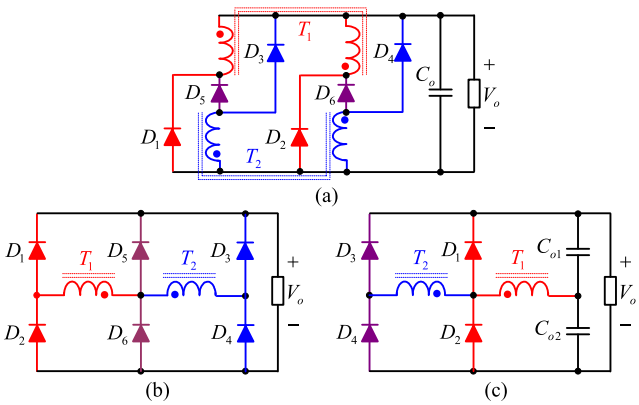

Fig. 3. Topology of hybrid rectifier, (a) center-tapped, (b) full-bridge, and (c) voltage-doubler.

secondary windings of the two transformers, T_1 and T_2. The *LLC* resonant switching network on the primary side is composed of a switching bridge and an *LLC* resonant network. As illustrated in Fig. 2, the switching-bridge can be a half-bridge, full-bridge, or three-level bridge.

The topology of the hybrid rectifier in the proposed iLLC resonant converter is shown in Fig. 3, where it is seen that the hybrid rectifier can be center-tapped type, full-bridge type, and voltage doubler type. Generally speaking, the center-tapped rectifier is suitable for applications with low output voltage and high-

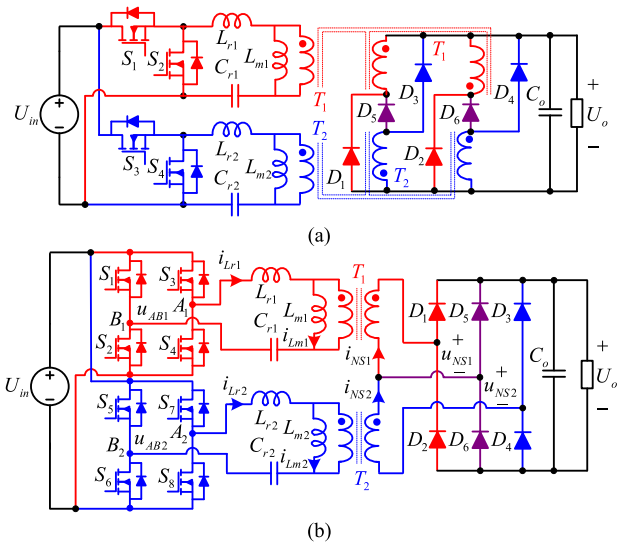

Fig. 4. Examples of iLLC resonant converter with hybrid rectifier, (a) half-bridge and (b) full-bridge.

output current, while the voltage doubler rectifier is suitable for applications with high output voltage. The two secondary windings in the proposed iLLC resonant converter can be connected in-series or not through the hybrid rectifier. The operation of the hybrid rectifier and connection of the two secondary windings are regulated by the phase-shift angle between the two *LLC* resonant switching networks on the primary side. Therefore, a new control freedom is provided by the iLLC and the hybrid rectifier. As a result, the output voltage can be regulated in a wide range without varying the switching frequency of the iLLC resonant converter.

A family of novel iLLC resonant converters can be harvested by replacing the block diagrams in Fig. 1 with corresponding circuits shown in Figs. 2 and 3, respectively. Two examples of iLLC resonant converter topology are shown in Fig. 4, where Fig. 4(a) is a half-bridge iLLC resonant converter with center-tapped hybrid rectifier, while Fig. 4(b) is a full-bridge iLLC resonant converter with a full-bridge hybrid rectifier.

III. Analysis on the Proposed Full-Bridge iLLC Resonant Converter

In this section, the full-bridge iLLC resonant converter shown in Fig. 4(b) is taken as an example to be analyzed to verify the operation principles and feasibility of the proposed method. Variable-frequency plus phase-shift (VFPPS) control is employed to the proposed iLLC resonant converter to regulate the output voltage in a wide output voltage range. Variable frequency control is adopted to regulate the output voltage and the secondary windings are in series when the output voltage is high. Fixed-frequency phase-shift control is adopted to regulate the output voltage by adaptively changing the connection of the two secondary windings when the output voltage is low. To simplify the analysis, the normalized voltage gain, G_i, is defined as

$$G_i = \frac{U_o}{NU_{\text{in}}} \tag{1}$$

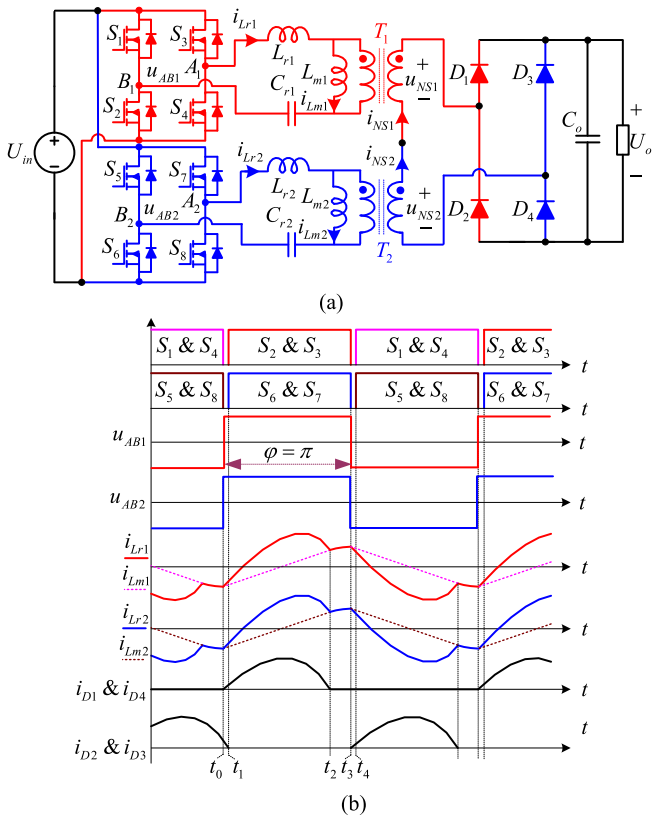

Fig. 5. Equivalent circuit and key waveforms in the variable-frequency mode, (a) equivalent circuit and (b) key waveforms.

where U_o and U_{in} are the output and input voltage, respectively, while N is the secondary to primary turns ratio of the transformers T_1 and T_2. The phase-shift angle φ is defined to be the phase difference between the gate signals of switch pairs S_2 & S_3 and S_5 & S_8. The control of the converter is achieved by varying the switching frequency f_S or the phase-shift angle φ.

A. Variable-Frequency Mode

When the iLLC converter operates in the variable-frequency mode, the switching frequency f_S is employed to regulate the output. f_S is lower than the resonant frequency, f_r, of the resonant tank and the phase-shift angle φ is kept at its maximum value, i.e., $\varphi = \pi$. Therefore, all the switches S_1–S_8 have the constant duty cycle of 0.5, the switches S_1, S_4, S_5 and S_8 are gated on/off simultaneously, while S_2, S_3, S_6 and S_7 are on/off simultaneously. In this mode, the voltages, u_{AB1} and u_{AB2}, produced by the switching bridges of the two *LLC* modules are always in phase. Therefore, the voltages, u_{NS1} and u_{NS2}, on the secondary windings of the two transformers T_1 and T_2 are in phase as well. It means the two secondary windings always operate in in-series manner. As a result, the rectifying bridge composed of D_5 and D_6 and shared by the two secondary windings does not work.

The equivalent circuit and key waveforms of the proposed iLLC resonant converter in the variable-frequency mode are illustrated in Fig. 5. It can be seen that the hybrid rectifier has degraded to be a conventional full-bridge rectifier. The iLLC

converter can be treated as a traditional variable-frequency modulated *LLC* resonant converter with split primary-side circuits and transformers. Therefore, the operation principles and waveforms of the iLLC resonant converter are the same as the conventional *LLC* resonant converter. The detailed operation principles in the variable-frequency mode will not be analyzed here.

It should be noted that the current flows through the resonant tanks and the transformer windings of the two *LLC* modules are always the same because the secondary windings are always in-series. Because of the primary-side parallel and secondary-winding series structure, the normalized voltage gain of the iLLC is two times of the normalized voltage gain G_{LLC} of each *LLC* module, i.e., $G_i = 2G_{LLC}$.

B. Fixed-Frequency Phase-Shift Mode

If the switching frequency f_S has been increased to f_r and the output voltage continuous to decrease, the iLLC resonant converter will enter the fixed-frequency phase-shift mode, in which f_S is kept at its maximum value, i.e., $f_S = f_r$, and the phase-shift angle φ is employed to regulate the output voltage. Since $\varphi < \pi$ and the voltages $u_{\rm AB1}$ and $u_{\rm AB2}$, and voltages $u_{\rm NS1}$ and $u_{\rm NS2}$ are not in phase, the connection of the secondary windings of T_1 and T_2 will be regulated by the polarity of $u_{\rm NS1}$ and $u_{\rm NS2}$. Since the two *LLC* modules operates at its resonant frequency, it is obvious that $G_i = 2$ if $\varphi = \pi$ and the two secondary windings work in in-series manner, whereas $G_i = 1$ if $\varphi = 0$ and the two secondary windings work in in-parallel manner. Therefore, by regulating the phase-shift angle φ and without increasing the switching frequency, the normalized voltage gain G_i can be regulated continuously between 1 and 2. As a result, the phase-shift angle can be used as a new control freedom to regulate the output voltage in a wide range, and the output voltage range regulated by the switching frequency mode can be narrowed significantly.

The *LLC* module composed of S_1–S_4 is defined as the lagging-module, while the *LLC* module composed of S_5–S_8 is defined as the leading-module. It means the gate signals of S_5–S_8 lead the corresponding gate signals of S_1–S_4.

1) Case I: $0 < \varphi < \pi$*:* The parameters of the two *LLC* modules are assumed to be the same. The key waveforms of the proposed iLLC converter with $0 < \varphi < \pi$ are shown in Fig. 6. It should be noted that the operation waveforms of the converter are only determined by the phase-shift angle and has nothing to do the transferred power. There are six switching stages in half-switching cycle. The equivalent circuit of each switching stage is shown in Fig. 7.

Stage I $[t_0, t_1]$ *[see Fig. 7(a)]:* Before t_0, switch pairs S_1 & S_4 and S_6 & S_7 are ON, all the diodes on the secondary side are OFF. At t_0, S_1 & S_4 are turned OFF, the body diodes of S_2 and S_3 are ON due to the negative resonant current i_{Lr1}. Meanwhile, the diodes D_1 and D_4 on the secondary side begin to conduct, because the polarities of voltages, $u_{\rm NS1}$ and $u_{\rm NS2}$, of the two secondary windings are the same. Therefore, the secondary windings operates in-series and the currents flow through the secondary windings, $i_{\rm NS1}$ and $i_{\rm NS2}$, are the same.

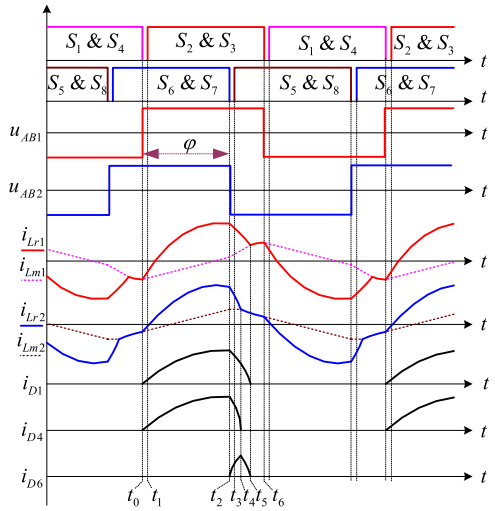

Fig. 6. Key waveforms of the iLLC converter in the phase-shift mode.

Stage II $[t_1, t_2]$ *[see Fig. 7(b)]:* At t_1, switches S_2 and S_3 are turned ON with zero voltage.

During Stages I and II, L_{r1} and L_{r2} resonate with C_{r1} and C_{r2}, respectively, and the currents of the two magnetizing inductors, L_{m1} and L_{m2}, increase linearly. The voltages applied on the two secondary windings

$$u_{\rm NS1} = u_{\rm NS2} = \frac{U_o}{2}. \tag{2}$$

Stage III $[t_2, t_3]$ *[see Fig. 7(c)]:* At t_2, the switches S_6 & S_7 are turned OFF, the body diodes of S_5 & S_8 are ON due to the positive current of i_{Lr2}. Then, the polarity of voltage $u_{\rm AB2}$ becomes negative. As a result, the diode D_6 begins to conduct due to the forward-biased voltage. According to the equivalent circuit shown in Fig. 7(c), when both D_6 and D_4 are ON, the secondary winding of T_2 is shorted and the current i_{Lr2} decreases rapidly. Hence, the two secondary windings are not in-series any more.

Stage IV $[t_3, t_4]$ *[see Fig. 7(d)]:* At t_3, the switches S_5 & S_8 are turned ON with zero-voltage.

During Stages III and IV, L_{r1} and L_{r2} resonate with C_{r1} and C_{r2}, respectively, but only the transformer T_1 transfers power to the output. The voltages $u_{\rm NS1}$ and $u_{\rm NS2}$ satisfy

$$\begin{cases} u_{\rm NS1} = U_o \\ u_{\rm NS2} = 0 \end{cases}. \tag{3}$$

Stage V $[t_4, t_5]$ *[see Fig. 7(e)]:* At t_4, the current $i_{\rm NS2}$ decreases to zero and the diode D_4 is OFF. $i_{\rm NS2}$ stays in zero in this stage because $U_o > G_{LLC}U_{\rm in}$. Therefore, L_{r2} and L_{m2} begin to resonate with C_{r2}. D_1 and D_6 are ON and only transformer T_1 supplies power to the load in this stage.

Stage VI $[t_5, t_6]$ *[see Fig. 7(f)]:* At t_5, the current $i_{\rm NS1}$ decreases to zero, and the diodes D_1 and D_6 are OFF. L_{r1} and L_{m1} begin to resonate with C_{r1}.

According to the operation principles, it is seen that the leading-module only transfers power to the load in the Stages I and II, while the lagging-module transfers power in Stages I–IV.

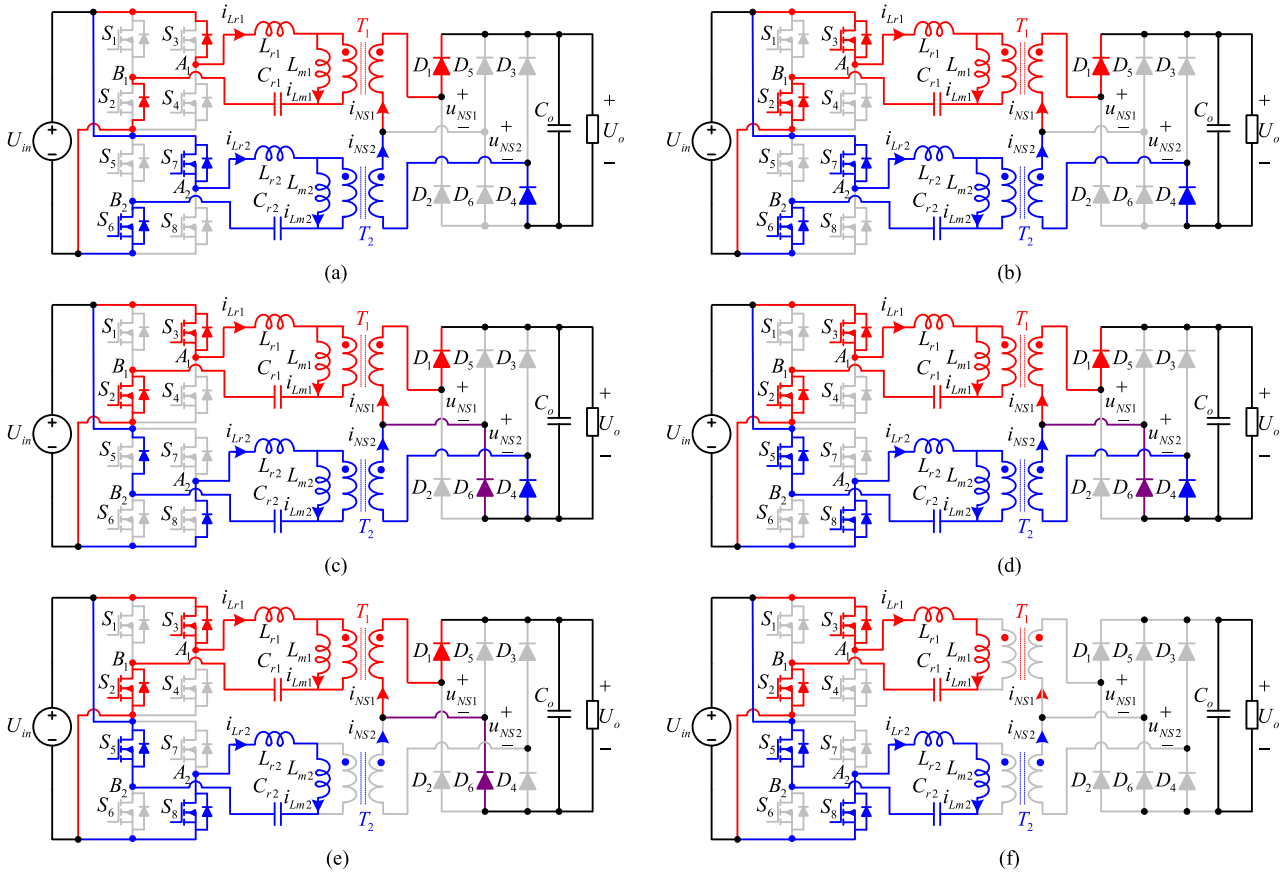

Fig. 7. Equivalent circuit of the phase-shift mode, (a) $[t_0, t_1]$, (b) $[t_1, t_2]$, (c) $[t_2, t_3]$, (d) $[t_3, t_4]$, (e) $[t_4, t_5]$, and (f) $[t_5, t_6]$.

Therefore, the transferred power of the two modules in the fixed-frequency mode is not the same. More specifically, the power ratio of the leading module decreases and the power ratio of the lagging module increases when the phase-shift angle decreases. From this point of view, the proposed converter is more suitable for the applications of battery charging for electric-vehicle and energy storage system, where the charging power decreases linearly with the decreasing of the battery voltage. In this case, even though the power ratio of the lagging-module is greater than the leading-module in the fixed-frequency mode, the power rating of the lagging module in the fixed-frequency mode is always lower than that in the variable-frequency mode, which means the power capacity of the iLLC converter is determined by the variable-frequency mode, rather than the phase-shift mode.

2) Case II: $\varphi = 0$: As analyzed above, the power ratio of the leading module in the fixed-frequency mode is proportional to the phase-shift angle φ. Therefore, when the phase-shift angle approaches to zero, the output power of the leading module will approach to zero as well. However, the situation will be changed once $\varphi = 0$, because the two modules will work in parallel when $\varphi = 0$. Theoretically, the current will be shared by the two modules if the parameters of the resonant tanks, transformers, switches, and diodes are all the same. However, in practice, it is very difficult to ensure the consistency of parameters. Considering that the output voltage and power is at its minimum value when $\varphi = 0$, and the fact that the output power of the leading module will approaches to zero when the phase-shift angle approaches to zero, one can shut down the leading module to avoid the current-sharing issue in the case of $\varphi = 0$. If the leading-module is turned OFF, the iLLC resonant converter will degrade to be a traditional full-bridge *LLC* resonant converter operating at its resonant frequency. The equivalent circuit and key waveforms of this situation are shown in Fig. 8. In this case, the operation principles are the same as the conventional *LLC* resonant converter. The detailed operation will not be analyzed here.

IV. Characteristics and Analysis

A. Voltage Gain

1) Variable-Frequency Mode: When the iLLC resonant converter operates in the variable-frequency mode, the voltage gain characteristic is the same as the conventional *LLC* resonant converter. Since the primary side of the two *LLC* modules are in-parallel while the secondary windings are in-series, the voltage gain of the iLLC resonant converter is two times of each *LLC* module, i.e., $G_i = 2G_{LLC}$. For simplicity, it is assumed that $L_{r1} = L_{r2} = L_r$ $L_{m1} = L_{m2} = L_m$. Using the fundamental harmonic analysis method [12], the voltage gain in the variable-frequency mode can be expressed as

$$G_i = \frac{U_o}{NU_{\text{in}}} = 2G_{\text{LLC}} = \frac{2}{\sqrt{\left[1+\frac{1}{k}\left(1-\frac{1}{f_N{}^2}\right)\right]^2 + Q_r{}^2\left(f_N - \frac{1}{f_N}\right)^2}} \quad (4)$$

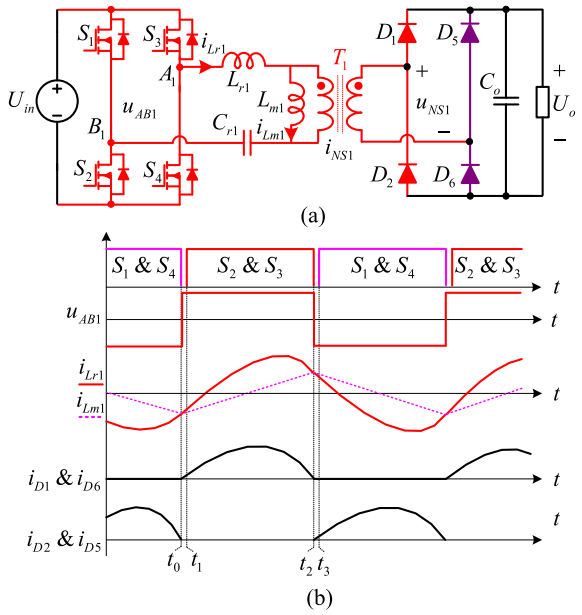

Fig. 8. Equivalent circuit and key waveforms when $\varphi = 0$ and the leading-module is turned off, (a) equivalent circuit and (b) key waveforms.

where

$$k = \frac{L_m}{L_r}, \quad f_N = \frac{f_S}{f_r} \tag{5}$$

$$f_r = \frac{1}{2\pi\sqrt{L_r C_r}} \tag{6}$$

$$Q_r = \frac{2N^2 Z_r}{R_o} \tag{7}$$

$$Z_r = \sqrt{\frac{L_r}{C_r}} \tag{8}$$

and R_o is the load resistance of the iLLC converter. It should be noted that the maximum switching frequency of the iLLC resonant converter is f_r, which means the iLLC will not enter the $f_S > f_r$ region, in which the rectifying diodes are hard switched.

2) Fixed-Frequency Phase-Shift Mode: When the iLLC converter works in the phase-shift mode, the switching frequency is fixed at f_r. It is obvious that the normalized voltage gain $G_i = 2$ if the phase-shift angle $\varphi = \pi$, while $G_i = 1$ if $\varphi = 0$. Therefore, it is easy to understand that the output voltage is proportional to the phase-shift angle φ, and the normalized voltage gain can be continuously regulated between 1 and 2 by varying φ between 0 and π. However, when the converter operates in the phase-shift mode, it is difficult to obtain a numerical solution for the voltage gain G_i because the multiple resonant stages will lead to a transcendental equation. In order to simplify the analysis and derive the relation between G_i and φ, the magnetizing inductance of the two transformers T_1 and T_2 are ignored in the following analysis.

In order to fully understand the voltage gain characteristic of the proposed iLLC resonant converter in the phase-shift mode, the steady-state trajectory curve of the resonant network composed of L_{r1} and C_{r1} is shown in Fig. 9, where the inductor

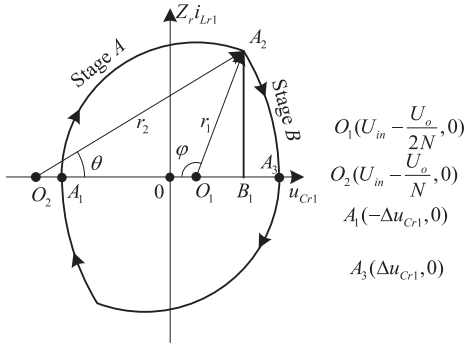

Fig. 9. Trajectory curve of state variables in the iLLC resonant converter.

current is multiplied by the impedance Z_r of the resonant tank. Seen from the trajectory curve, the Stages I and II in the phase-shift mode can be simplified to the Stage A in Fig. 9. During the Stage A, U_{in} supplies power to the load through both the two transformers T_1 and T_2, the secondary windings of T_1 and T_2 are connected in series, and the converter moves along the trajectory curve from point A_1 to A_2. The center point O_1 around which the L_{r1} and C_{r1} resonate is located at $(U_{\text{in}} - \frac{U_o}{2N}, 0)$, and the i_{Lr1} and u_{Cr1} are expressed as follows:

$$i_{Lr1}(t) = \frac{r_1}{Z_r}\sin[\omega_r(t - t_0)] \tag{9}$$

$$u_{Cr1}(t) = \left(U_{\text{in}} - \frac{U_o}{2N}\right) - r_1\cos[\omega_r(t - t_0)] \tag{10}$$

where $\omega_r = 2\pi f_r$ and the radius r_1 of the trajectory curve

$$r_1 = U_{\text{in}} - \frac{U_o}{2N} + \Delta u_{Cr1} \tag{11}$$

$$\Delta u_{Cr1} = \frac{P_1}{4U_{\text{in}} f_s C_r} \tag{12}$$

P_1 is the average output power transferred by the transformer T_1.

When the switches S_6 & S_7 are turned OFF at t_2, the converter enters the resonant Stage B in Fig. 9, during which only the transformer T_1 supplies power to the load. In the Stage B, the converter moves along the trajectory curve from point A_2 to A_3. The center point O_2 around which the L_{r1} and C_{r1} resonate is located at $(U_{\text{in}} - \frac{U_o}{N}, 0)$, and the i_{Lr1} and u_{Cr1} are expressed as follows:

$$i_{Lr1}(t) = \frac{r_2}{Z_r}\sin[\theta - \omega_r(t - t_2)] \tag{13}$$

$$u_{Cr1}(t) = \left(U_{\text{in}} - \frac{U_o}{N}\right) + r_2\cos[\theta - \omega_r(t - t_2)]. \tag{14}$$

The radius r_2 of the trajectory curve

$$r_2 = \frac{U_o}{N} - U_{\text{in}} + \Delta u_{Cr1}. \tag{15}$$

According to (9)–(15), the following equation is satisfied at t_2:

$$i_{Lr1}(t_2) = \frac{r_1}{Z_r}\sin\varphi = \frac{r_2}{Z_r}\sin\theta. \tag{16}$$

Therefore the phase-shift angle θ is derived as

$$\theta = \arcsin\left(\frac{r_1}{r_2}\sin\varphi\right). \tag{17}$$

According to the operation principles of the iLLC resonant converter in the phase-shift mode, the leading *LLC* module only transfers power to the load during the resonant Stage A, while the lagging *LLC* module transfers power to the load during the resonant Stages A and B. Therefore, the average output power transferred by the transformer T_1 is

$$P_1 = U_o \frac{\int_0^{t_5} i_{Lr1}(t)dt}{NT_S/2}. \tag{18}$$

In the resonant Stage A, the secondary windings of the two transformers are connected in series and transfer power to the load simultaneously. Therefore, if the magnetizing current of the two transformers is ignored for simplicity, the resonant current of the two modules should be the same, i.e., $i_{Lr1} = i_{Lr2}$, even though the voltages of the two resonant capacitors are not the same. Therefore, the average output power transferred by the transformer T_2 is calculated as follows:

$$P_2 = U_o \frac{\int_0^{t_2} i_{Lr1}(t)dt}{NT_S/2}. \tag{19}$$

Ignoring the power conversion losses, the output power can be calculated as

$$P_o = P_1 + P_2 = \frac{U_o^2}{R_o} \tag{20}$$

where R_o is the load resistance. Substituting (1) and (9)–(19) into (20), the following equation is derived:

$$\pi Q_r\left[2-\left(\sin\frac{\varphi}{2}\right)^2\right]{G_i}^3 + \left[6\left(\sin\frac{\varphi}{2}\right)^2 - 2\pi Q_r\right]{G_i}^2$$
$$-16\left(\sin\frac{\varphi}{2}\right)^2 G_i + 8\left(\sin\frac{\varphi}{2}\right)^2 = 0. \tag{21}$$

According to (21), the relationship between the normalized voltage gain G_i and the phase-shift angle φ is given by

$$\varphi = \arcsin\left(G_i\sqrt{\frac{2\pi Q_r(G_i-1)}{\pi Q_r {G_i}^3 - 6G_i^2 + 16G_i - 8}}\right). \tag{22}$$

Based on (4) and (22), the voltage gain curves of the proposed iLLC resonant converter are shown in Fig. 10. The curves of variable-frequency control are plotted with $k = 8$. Fig. 10(a) is the voltage gain curves of the iLLC resonant converter with the VFPPS control. It can be seen that the output voltage can be regulated in a wide range with a very narrow switching-frequency range. $G_i = 2$ when $f_S = f_r$ and $\varphi = \pi$. The converter operations in the variable-frequency mode and the switching frequency $f_S < f_r$ when $G_i > 2$, whereas f_S stays at f_r and the converter operates in the phase-shift mode when $G_i < 2$. The comparison between the phase-shift control and the traditional variable frequency control is illustrated in Fig. 10(b). It is seen that the normalized voltage gain drops slowly in the $f_S > f_r$ region. For example, G_i only decreases to 1.7 when $Q_r = 0.2$ and f_S has increased to two times of the resonant frequency f_r. It means a much higher switching frequency is needed to obtain

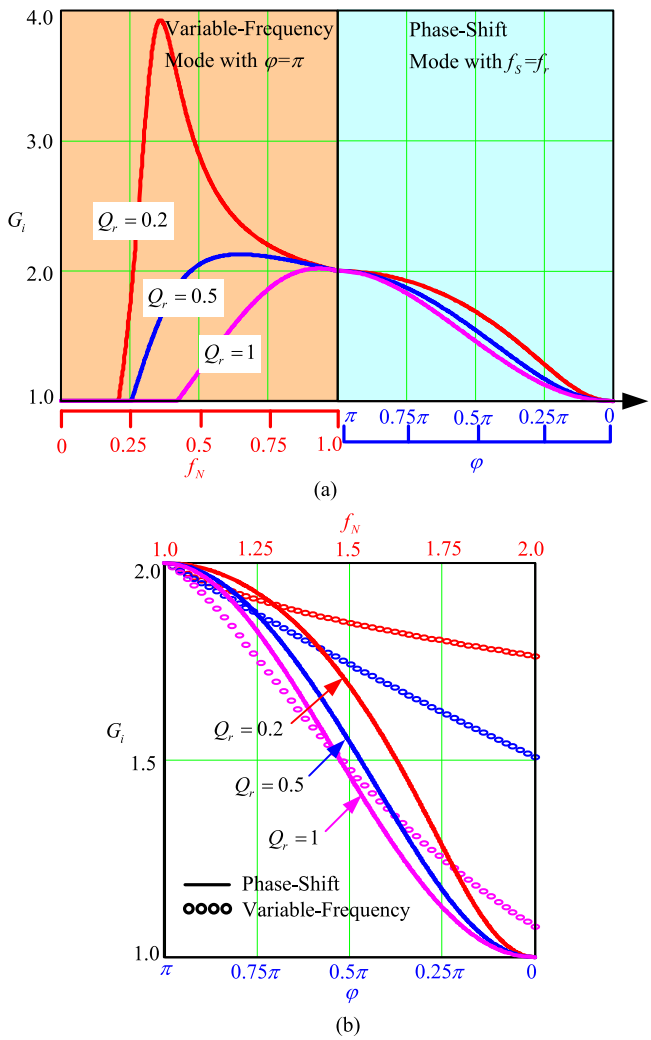

Fig. 10. Voltage gain curves, (a) voltage gain of the proposed iLLC converter and (b) comparison between phase-shift control and variable frequency control.

the same output voltage range if only variable frequency control is employed. In addition, it can be seen that the voltage regulation of phase-shift control is not sensitive to the output load, i.e., the quality factor Q_r, whereas the variable frequency is very sensitive to Q_r. That is why the conventional *LLC* resonant converter is difficult to control under light load condition.

B. Soft-Switching Performance

According to the operation principles, it is seen that zero-voltage turn-on and zero-current off can be achieved for all the active switches and rectifying diodes in both variable-frequency and phase-shift modes. Therefore, excellent soft-switching performance within the entire operation range can be achieved with the proposed iLLC resonant converter as well, which is the same as the conventional *LLC* resonant converter. Meanwhile, another advantage of the proposed iLLC resonant converter in comparison with the traditional *LLC* resonant converter is that the switching-frequency range of the resonant tank is reduced. Therefore, the output voltage can be regulated in a wide range without varying the switching frequency in a wide range. Meanwhile, since the operation range of the variable-frequency mode

is narrowed, the circulating current and the additional conduction losses associated with the magnetizing inductance can be reduced as well.

C. Circulating Current Analysis

The advantage of excellent soft-switching performance of traditional *LLC* resonant converter has been maintained by the proposed iLLC converter. However, it should be noted that, the iLLC converter still has some drawbacks when it operates in the phase-shift mode. According to the operation principles in the phase-shift mode, in the Stages III and IV of the phase-shift mode, the secondary winding of T_2 is shorted and the current i_{Lr2} is recycled to the input instead of transferred to the output. Therefore, the current of i_{Lr2} in the Stages III and IV represents a circulating current, which will lead to additional conduction loss. According to the waveform of resonant current i_{Lr2}, the circulating current increases as the phase-shift angle φ approaches to $\pi/2$, and decreases when φ approaches to 0 or π. Hence, it can be estimated that, when the iLLC operates in the phase-shift mode, the conversion efficiency decreases when the phase-shift angle φ increases from 0 to $\pi/2$, and the efficiency would increase when the phase-shift angle φ increases from $\pi/2$ to π.

V. Experimental Evaluation and Analysis

A 3.5 kW experimental prototype is built based on the proposed full-bridge iLLC resonant converter to evaluate the performance of the proposed iLLC resonant converter and its control strategies. The input voltage $U_{\rm in} = 400\ {\rm V} \pm 10\ {\rm V}$, output voltage $U_o = 150$–500 V, the maximum output current $I_{\rm omax} = 7$ A. To fully utilize the output voltage regulation capability of the phase-shift mode, the turns ratio of the two transformers is designed to be $N = 3{:}8$, in which case the output voltage range of the variable frequency mode is 300–500 V while the output voltage range of the fixed-frequency phase-shift mode is 150–300 V. The output voltage $U_o = 300$ V when $f_S = f_r$ and $\varphi = \pi$, and $U_o = 150$ V when $\varphi = 0$. The resonant frequency f_r of the resonant tank in the iLLC converter is 100 kHz. The devices' parameters in the prototype are as follows. $L_{r1} = 53.8\,\mu$H, $L_{r2} = 53.9\,\mu$H, $C_{r1} = C_{r2} = 47$ nF, $L_{m1} = L_{m2} = 430\,\mu$H, S_1–S_8: IXFH22N60P, D_1–D_6: DSEK60-06A.

The steady-state experimental waveforms when $U_o = 500$ V are shown in Fig. 11. Fig. 11(a) is the waveforms of the primary-side voltages $u_{\rm AB1}$, $u_{\rm AB2}$ and currents i_{Lr1} and i_{Lr2}, whereas Fig. 11(b) is the waveforms of the secondary-side voltages $u_{\rm NS1}$, $u_{\rm NS2}$ and currents $i_{\rm NS1}$ and $i_{\rm NS2}$. When the output voltage U_o is 500 V, the iLLC resonant converter operates in the variable-frequency mode with $f_S < f_r$. It is seen that the waveforms of i_{Lr1} and i_{Lr2} are the same as that in a traditional variable-frequency modulated *LLC* resonant converter. Meanwhile, since the phase-shift angle φ is kept at its maximum value, i.e., $\varphi = \pi$, the two secondary windings of the two transformers are always connected in series. Therefore, as shown in the experimental waveforms, the voltages $u_{\rm AB1}$ and $u_{\rm AB2}$, and the voltages $u_{\rm NS1}$ and $u_{\rm NS2}$ are always in phase. The currents i_{Lr1} and i_{Lr2} are equal, while $i_{\rm NS1}$ and $i_{\rm NS2}$ are equal, which means the output power is shared equally by the two *LLC* modules and two transformers.

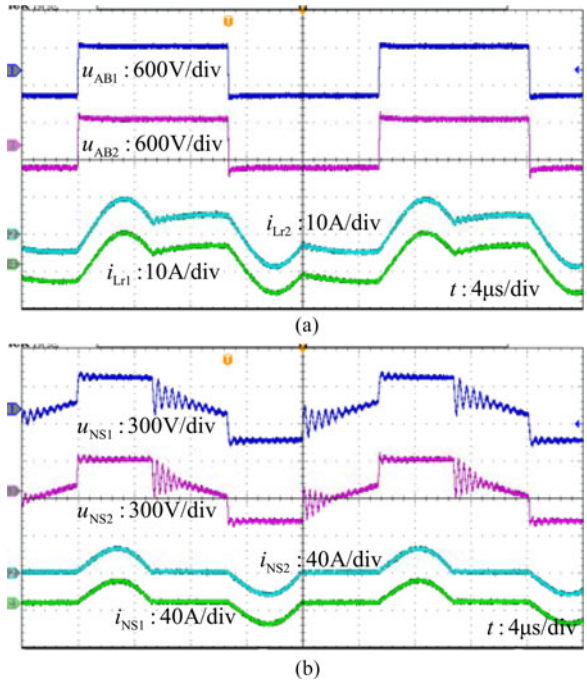

Fig. 11. Switching waveforms at $U_o = 500$ V, (a) $u_{\rm AB1}$, $u_{\rm AB2}$, i_{Lr1} and i_{Lr2} and (b) $u_{\rm NS1}$, $u_{\rm NS2}$, $i_{\rm NS1}$ and $i_{\rm NS2}$.

The steady-state waveforms when $U_o = 300$ V are shown in Fig. 12, where the iLLC resonant converter works in the boundary of variable-frequency mode and phase-shift mode with $f_S = f_r$ and $\varphi = \pi$. Fig. 12(a) is the waveforms of primary-side voltages $u_{\rm AB1}, {\rm u_{AB2}}$ and currents $i_{Lr1}, {\rm i_{Lr2}}$, Fig. 12(b) is the waveforms of secondary-side voltages $u_{\rm NS1}, {\rm u_{NS2}}$ and currents $i_{\rm NS1}, {\rm i_{NS2}}$. Fig. 12(c) is the soft-switching waveforms of the primary-side switch S_2. It is seen that the switching frequency equals to the resonant frequency. $u_{\rm AB1}$, i_{Lr1}, ${\rm u_{NS1}}$, and $i_{\rm NS1}$ are in phase with $u_{\rm AB2}, {\rm i_{Lr2}}, u_{\rm NS2}$,and $i_{\rm NS2}$, respectively, which indicates that the two secondary windings of the two transformers T_1 and T_2 work in series and the output power is shared equally by the two *LLC* modules. The waveforms shown in Fig. 12(c) indicate that soft-switching of the primary side switch is achieved.

The steady-state waveforms when $U_o = 250$ V are shown in Fig. 13, where the iLLC resonant converter works in the fixed-frequency phase-shift mode. Fig. 13(a) and (b) are tested at full-load condition, while Fig. 13(c) and (d) are tested at half-load condition. It is seen that the voltage $u_{\rm AB1}$ produced by the switches S_1–S_4 lags the voltage $u_{\rm AB2}$ produced by the switches S_5–S_8. From the current waveforms of i_{Lr1}, i_{Lr2}, $i_{\rm NS1}$ and $i_{\rm NS2}$, it can be seen that the resonant inductors $L_{\rm r1}$ and L_{r2} begin to resonate with the capacitors C_{r1} and C_{r2} when the lagging voltage $u_{\rm AB1}$ commutates. When the two secondary windings works in in-series mode, the current $i_{\rm NS1}$ and $i_{\rm NS2}$ are the same, which means the two transformers supply power to the load simultaneously. When the leading voltage $u_{\rm AB2}$ commutates, the voltage $u_{\rm NS2}$ is zero in a short interval, which means the secondary winding of T_2 is shorted by the hybrid rectifier. It should be noted that the voltage rings on the secondary winding $u_{\rm NS1}$ and $u_{\rm NS2}$ are induced by the resonance between the leakage inductance of

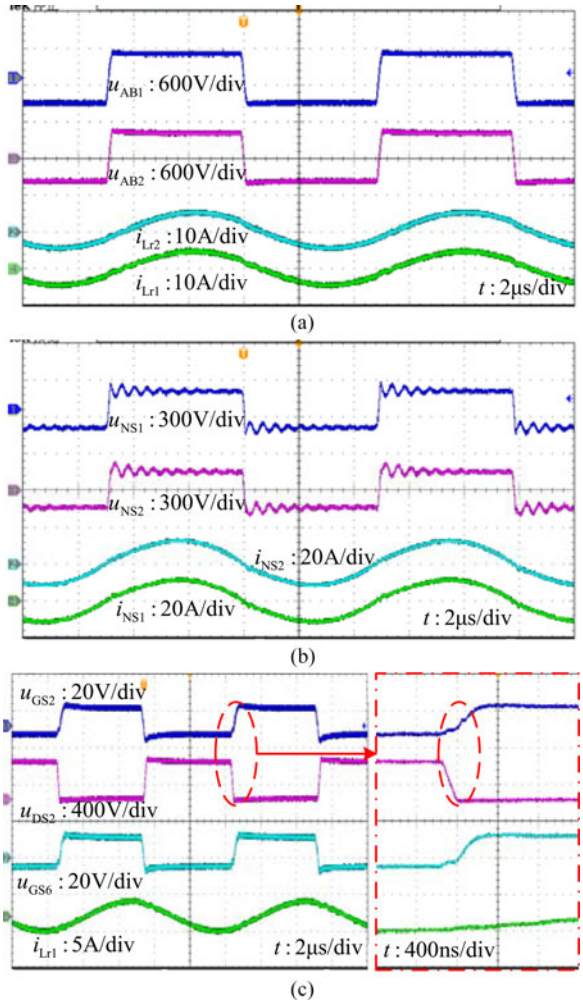

Fig. 12. Switching waveforms at $U_o = 300$ V, (a) $u_{\mathrm{AB1}}, u_{\mathrm{AB2}}, i_{Lr1}$ and i_{Lr2}, (b) u_{NS1}, u_{NS2}, i_{NS1} and i_{NS2}, and (c) u_{GS2}, u_{DS2}, u_{GS6} and i_{Lr1}.

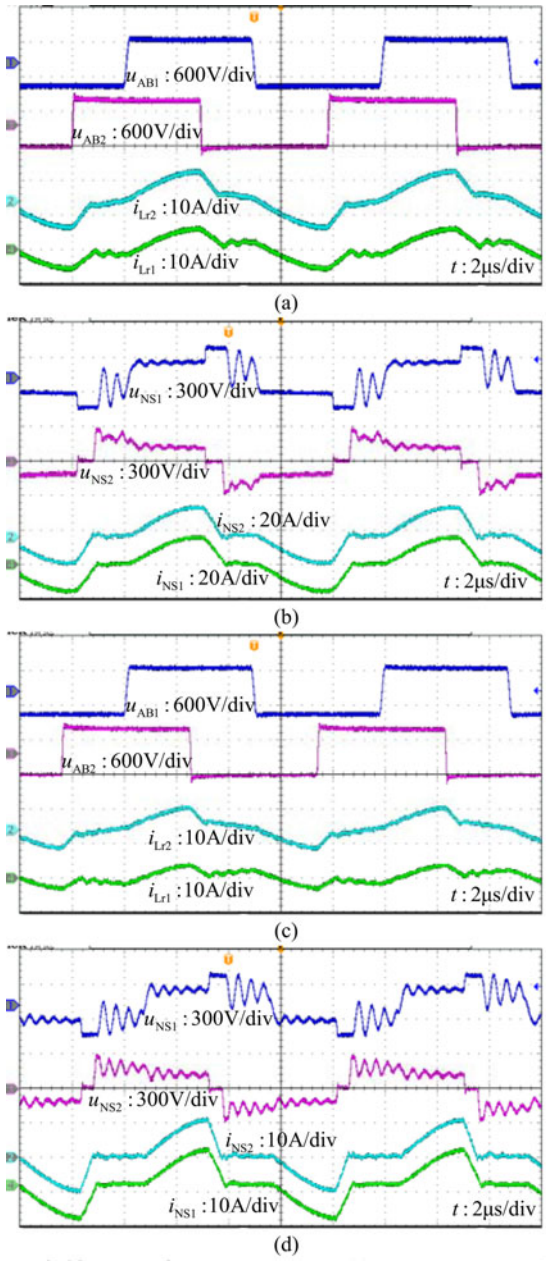

Fig. 13. Switching waveforms at $U_o = 250$ V, (a) $u_{\mathrm{AB1}}, u_{\mathrm{AB2}}, i_{Lr1}$ and i_{Lr2} at full-load, (b) u_{NS1}, u_{NS2}, i_{NS1} and i_{NS2} at full-load, (c) u_{AB1}, u_{AB2}, i_{Lr1} and i_{Lr2} at half-load, and (d) u_{NS1}, u_{NS2}, i_{NS1} and i_{NS2} at half-load.

transformers and the parasitic capacitance of the diodes D_5 and D_6 in the hybrid rectifier. In addition to the voltage rings of u_{NS1} and u_{NS2}, the experimental waveforms coincide with the theoretical analysis pretty well. Meanwhile, it is seen that the waveforms with half-load are similar to the waveforms with full-load, and the phase-shift angle under half-load is slightly lower than that under full-load, which indicates that the phase-shift angle is proportional to the output load but not sensitive to the output load. This feature can be observed from the voltage gain curves shown in Fig. 10 as well.

When the converter operates in the phase-shift mode, the ZVS waveforms of the switch S_2 in the lagging module and the switch S_6 in the leading module are shown Fig. 14(a) and (b), respectively. It is seen that ZVS has been achieved for both the switches in the leading module and lagging module. Since the switches S_1–S_4 operate in a symmetrical manner, so do switches S_5–S_8. It is proven that ZVS is achieved for all the primary-side switches.

The ZCS waveforms of the rectifying diodes in the leading module are tested and shown in Fig. 15, where Fig. 15(a) is tested in the variable-frequency mode with $f_s < f_r$, while Fig. 15(b) are tested in the fixed-frequency mode. It is seen that ZCS of the rectifying diodes, D_4 and D_6, have been achieved in the fixed-frequency mode. However, the ZCS waveforms in the fixed-frequency mode are not as good as that in the variable-frequency mode. It is because the current slew rate in the fixed-frequency mode is faster than that in the variable-frequency mode when the diodes' current decrease to zero. Therefore, a very slight reverse current is observed from Fig. 15(b). However, since the current slew rate is always limited by the resonant inductor, the reverse current and its related loss is very low.

The voltage gain curves of the proposed iLL resonant converter in the fixed-frequency mode are tested and compared with the theoretical analysis, as shown in Fig. 16. It is seen that the trend of the tested voltage gain curves coincides with the

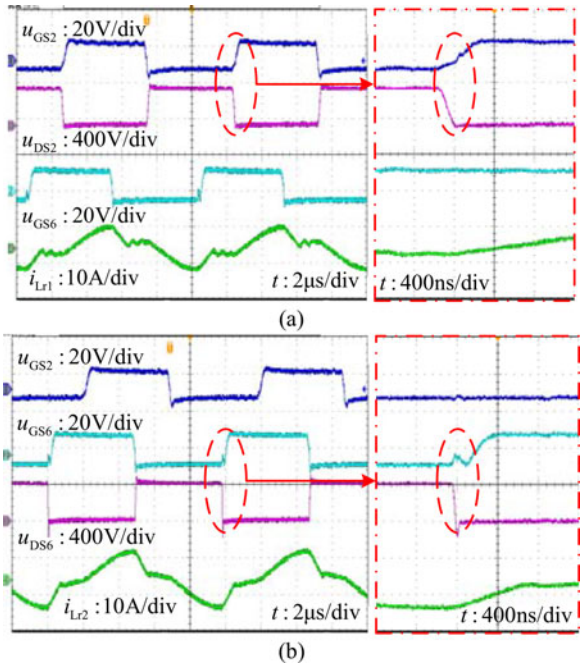

Fig. 14. Soft-switching waveforms at the phase-shift mode, (a) u_{GS2}, u_{DS2}, u_{GS6} and i_{Lr1} and (b) u_{GS2}, u_{GS6}, u_{DS6} and i_{Lr2}.

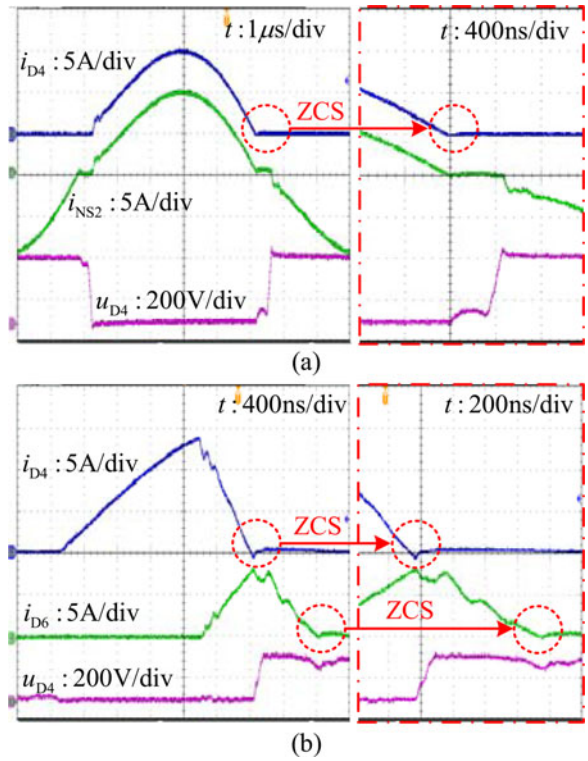

Fig. 15. ZCS waveforms of the rectifying diode in the leading-module, (a) variable-frequency mode and (b) fixed frequency mode.

theoretical analysis very well. However, the tested voltage gain is lower than the calculated results. The main reason is that the real quality factor Q_r is greater than the theoretical one. In theoretical analysis, the load resistance is directly reflected to the primary side and used to calculate the quality factor Q_r, but the real equivalent load resistance reflected to the resonant tank is lower than the load resistance.

The dynamic waveforms with load step-up and step-down in the phase-shift mode are shown in Fig. 17. It can be seen that the output voltage is stable when load steps-up/down, which indicates a good output voltage regulation performance of the phase-shift control.

The efficiency curves of the proposed full-bridge iLLC resonant converter are shown in Fig. 18. The curves in Fig. 18(a) are tested under different output current. It is seen that efficiency greater than 96% has been achieved in a wide load range when output voltage varies from 500 to 150 V, the highest efficiency is up to 98%, and the best efficiency curve is obtained when $U_o = 300\,\mathrm{V}$ with $f_S = f_r$ and $\varphi = \pi$. It is because that both the switching losses and conduction losses are minimized at the boundary of variable-frequency and phase-shift modes. The efficiency curves with respect to output voltage are shown in Fig. 18(b). It is seen that a very flat efficiency curve is achieved when the converter works with full load and in the variable-frequency mode. It is because a wide output voltage range is covered by the phase-shift mode, and the output voltage regulation range is narrowed. Therefore, the conduction losses associated with the magnetizing inductance of transformers are reduced. However, the influence of the circulating current associated with the magnetizing inductance is very clear when the converter works at light load condition. As shown in Fig. 18(b), the efficiency

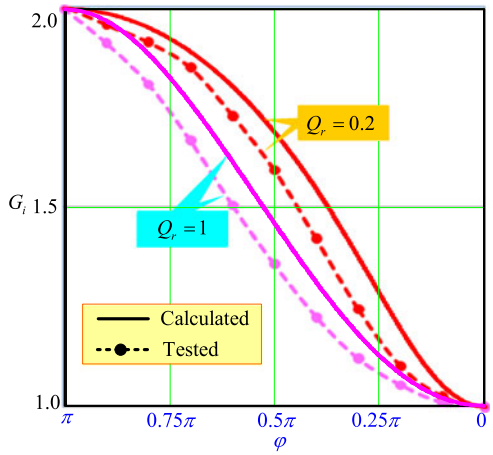

Fig. 16. Voltage gain curves of the iLLC converter in the fixed-frequency mode.

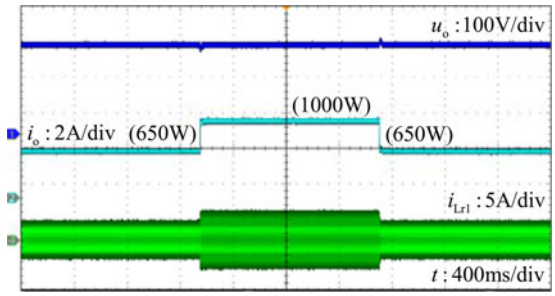

Fig. 17. Experimental waveforms with load step-up/down in the phase-shift mode.

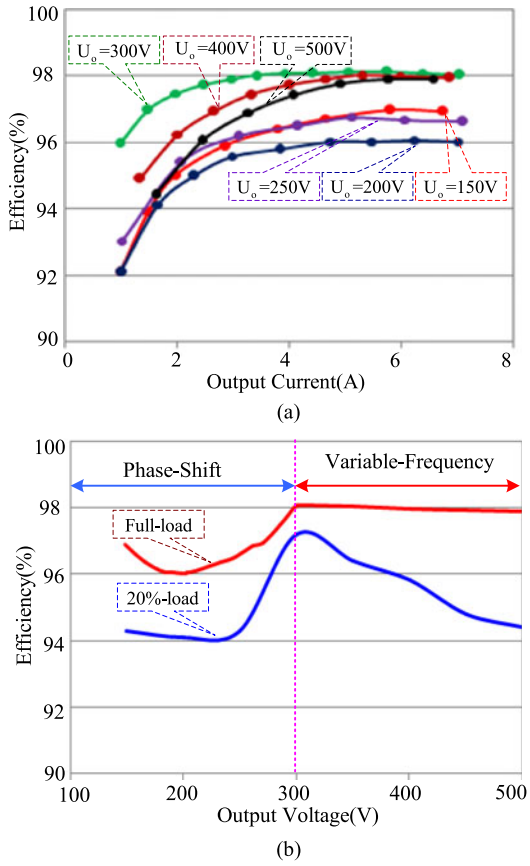

Fig. 18. Efficiency curves, (a) efficiency versus output current and (b) efficiency versus output voltage.

curve at 20% load in the variable frequency mode drops rapidly when the output voltage increases.

The efficiency curves shown in Fig. 18(b) indicate that with the decreasing of output voltage, the trend of efficiency curves in the phase-shift mode is first falling then rising. As analyzed above, the current of $i_{\mathrm{Lr}2}$ in the Stages III and IV of the phase-shift mode represents a circulating current, which will lead to additional conduction loss. The circulating current increases as the phase-shift angle φ approaches to $\pi/2$, and decreases when φ approaches to 0 or π. Therefore, the circulating current reach its maximum value when $\varphi = \pi/2$. As a result, the conduction loss and turned-OFF loss of the switches in the leading module reach their maximum values when $\varphi = \pi/2$ as well. That is why the trend of efficiency curves in the phase-shift mode is first falling then rising. From the efficiency curves, it is seen that the efficiency in the phase-shift mode is lower than that in the variable-frequency mode. However, if the output voltage range of variable-frequency mode is extended, the overall efficiency of the variable-frequency mode will decrease as well. For example, in comparison with the variable-frequency controlled improved *LLC* resonant converters in [18]–[20], the conversion efficiency of the proposed iLLC resonant converter is still higher, even when the converter operates in the fixed-frequency mode. In practice, the operation voltage range and the conversion efficiency of the variable-frequency mode are contradictory. A tradeoff between the operation voltage range and the overall

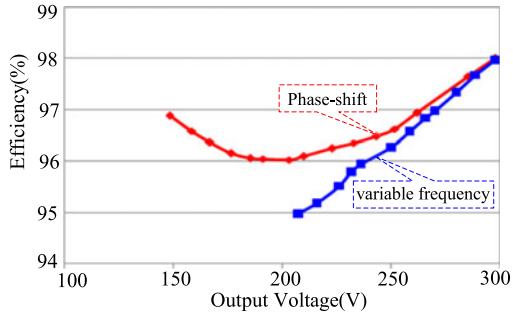

Fig. 19. Efficiency comparison.

conversion efficiency must be made for the variable-frequency mode. Nevertheless, the proposed iLLC resonant converter and the phase-shift control provide a new control freedom for the traditional *LLC* resonant converter. The output voltage range of the variable frequency mode can be narrowed significantly by introducing the phase-shift control.

The main objective of this research is providing a new voltage regulation method and extending the voltage gain range of the *LLC* resonant converter without pushing the switching frequency into the $f_s > f_r$ region. Fig. 19 shows the efficiency comparison results between the proposed control method and the variable-frequency control at full-load condition. For the variable-frequency control, the current is always shared by the two modules, but the switching frequency must be higher than f_r when the output voltage is lower than 300 V. It is obvious that the lower the output voltage is, the more obvious the advantage of the proposed fixed-frequency control is. In our test, the switching frequency has been up to 2.5 times of f_r when the output voltage is 200 V. Therefore, the efficiency of variable-frequency control with output voltage lower than 200 V is not tested any more.

VI. Conclusion

iLLC resonant converters with hybrid rectifier and VFPPS control are proposed for wide output voltage range applications. Theoretical analysis and experimental results indicate that a new control freedom is provided and the output voltage can be regulated in a wide range by employing phase-shifting control between the two iLLC modules. The connection of the transformers' secondary windings of the two *LLC* modules can be regulated with help of the hybrid rectifier and fixed-frequency phase-shift control. In addition, ZVS of primary-side switches and ZCS of secondary-side rectifying diodes can be always achieved. The advantages of variable frequency control and phase-shift control are combined. Therefore, in comparison with the traditional variable-frequency controlled *LLC* resonant converter, the switching frequency range of the proposed iLLC resonant converter is narrowed significantly. Hence, the circulating current and additional conduction losses associated with the magnetizing inductance of the *LLC* resonant converter is reduced dramatically. As a result, the contradiction between efficiency and voltage range of *LLC* resonant converters is solved. Effectiveness and feasibility of the proposed solution has been

evaluated and verified by experimental results on a 3.5 kW prototype with 400 V input voltage and 150–500 V output voltage.

REFERENCES

[1] Z. Hu, Y. Qiu, L. Wang, and Y.-F. Liu, "An interleaved LLC resonant converter operating at constant switching frequency," *IEEE Trans. Power Electron.*, vol. 29, no. 6, pp. 2931–2943, Jun. 2014.

[2] I. Demirel and B. Erkmen, "A very low-profile dual output LLC resonant converter for LCD/LED TV applications," *IEEE Trans. Power Electron.*, vol. 29, no. 7, pp. 3514–3524, Jul. 2014.

[3] M. A. Saket, N. Shafiei, M. Ordonez, M. Craciun, and C. Botting, "Low parasitics planar transformer for LLC resonant battery chargers," in *IEEE Appl. Power Electron. Conf. Expo.*, 2016, pp. 854–858.

[4] G. Yang, P. Dubus, and D. Sadarnac, "Double-phase high-efficiency, wide load range high-voltage/ low-voltage LLC DC/DC converter for electric/hybrid vehicles," *IEEE Trans. Power Electron.*, vol. 30, no. 4, pp. 1876–1886, Apr. 2015.

[5] X. Sun, Y. Shen, Y. Zhu, and X. Guo, "Interleaved boost-integrated LLC resonant converter with fixed-frequency PWM control for renewable energy generation applications," *IEEE Trans. Power Electron.*, vol. 30, no. 8, pp. 4312–4326, Aug. 2015.

[6] C.-H. Chang, C.-A. Cheng, and H.-L. Cheng, "Modeling and design of the LLC resonant converter used as a solar-array simulator," *IEEE J. Emerging Sel. Topics Power Electron.*, vol. 2, no. 4, pp. 833–841, Dec. 2014.

[7] H. Wang, Y. Chen, Y.-F. Liu, J. Afsharian, and Z. Yang, "A new LLC converter family with synchronous rectifier to increase voltage gain for hold-up applications," in *IEEE Energy Convers. Congr. Expo.*, 2015, pp. 5447–5453.

[8] Z. Hu, L. Wang, H. Wang, Y.-F. Liu, and P. C. Sen, "An accurate design algorithm for LLC resonant converters-part I," *IEEE Trans. Power Electron.*, vol. 31, no. 8, pp. 5435–5447, Aug. 2016.

[9] F. Musavi, M. Craciun, D. S. Gautam, W. Eberle, and W. G. Dunford, "An LLC resonant DC-DC converter for wide output voltage range battery charging applications," *IEEE Trans. Power Electron.*, vol. 28, no. 12, pp. 5437–5445, Dec. 2013.

[10] Z. Fang, T. Cai, S. Duan, and C. Chen, "Optimal design methodology for LLC resonant converter in battery charging applications based on time-weighted average efficiency," *IEEE Trans. Power Electron.*, vol. 30, no. 10, pp. 5469–5483, Oct. 2015.

[11] R. Yu, G. K. Y. Ho, B. M. H. Pong, B. W.-K. Ling, and J. Lam, "Computer-aided design and optimization of high-efficiency LLC series resonant converter," *IEEE Trans. Power Electron.*, vol. 27, no. 7, pp. 3243–3456, Jul. 2012.

[12] R. Beiranvand, B. Rashidian, M. R. Zolghadri, and S. M. H. Alavi, "A design procedure for optimizing the LLC resonant converter as a wide output range voltage source," *IEEE Trans. Power Electron.*, vol. 27, no. 8, pp. 3749–3763, Aug. 2012.

[13] W. Feng, F. C. Lee, and P. Mattavelli, "Optimal trajectory control of burst mode for LLC resonant converter," *IEEE Trans. Power Electron.*, vol. 28, no. 1, pp. 457–466, Jan. 2013.

[14] S. Zhao, J. Xu, and O. Trescases, "Burst-mode resonant LLC converter for an LED luminaire with integrated visible light communication for smart buildings," *IEEE Trans. Power Electron.*, vol. 29, no. 8, pp. 4392–4402, Aug. 2014.

[15] N. Shafiei, M. Ordonez, M. Craciun, C. Botting, and M. Edington, "Burst mode elimination in high-power LLC resonant battery charger for electric vehicles," *IEEE Trans. Power Electron.*, vol. 31, no. 2, pp. 1173–1188, Feb. 2016.

[16] J.-H. Kim, C.-E. Kim, J.-K. Kim, J.-B. Lee, and G.-W. Moon, "Analysis on load-adaptive phase-shift control for high efficiency full-bridge LLC resonant converter under light-load conditions," *IEEE Trans. Power Electron.*, vol. 31, no. 7, pp. 4942–4955, Jul. 2016.

[17] H. Wu, T. Mu, X. Gao, and Y. Xing, "A secondary-side phase-shift-controlled LLC resonant converter with reduced conduction loss at normal operation for hold-up time compensation application," *IEEE Trans. Power Electron.*, vol. 30, no. 10, pp. 5352–5357, Oct. 2015.

[18] Z. Liang, R. Guo, G. Wang, and A. Huang, "A new wide input range high efficiency photovoltaic inverter," in *Proc. IEEE Energy Convers. Congr. Expos.*, 2010, pp. 2937–2943.

[19] H. Hu, X. Fang, F. Chen, Z. J. Shen, and I. Batarseh, "A modified high-efficiency LLC converter with two transformers for wide input-voltage range applications," *IEEE Trans. Power Electron.*, vol. 28, no. 4, pp. 1946–1960, Apr. 2013.

[20] H. Wu, Y. Li, and Y. Xing, "LLC resonant converter with semiactive variable-structure rectifier (SA-VSR) for wide output voltage range application," *IEEE Trans. Power Electron.*, vol. 31, no. 5, pp. 3389–3394, May 2016.

[21] P. Sun, L. Zhou, and K. Ma, "A reconfigurable structure DC-DC converter with wide output range and constant peak power," *IEEE Trans. Power Electron.*, vol. 26, no. 10, pp. 2925–2935, Oct. 2011.

[22] X. Wu, H. Chen, J. Zhang, F. Peng, and Z. Qian, "Interleaved phase-shift full-bridge converter with transformer winding series-parallel autoregulated (SPAR) current doubler rectifier," *IEEE Trans. Power Electron.*, vol. 30, no. 9, pp. 4864–4873, Sep. 2015.

[23] G. Zhang, X. Wu, W. Yuan, J. Zhang, and Z. Qian, "A new interleaved active-clamp forward converter with parallel input and series-parallel output," in *24th Annu. IEEE Appl. Power Electron. Conf. Expo.*, 2009, pp. 40–44.

[24] X. Wu and H. Chen, "Two-phase hybrid forward convertor with series-parallel auto-regulated transformer windings and a common output inductor," *J. Power Electron.*, vol. 13, no. 5, pp. 757–765, 2013.

[25] H. Chen, X. Wu, C. Hu, and M. Chen, "A hybrid ZVS full-bridge converter with transformer winding series-parallel auto regulated current doubler rectifier," *IEEE Energy Conserv. Congr. Expo.*, 2012, pp. 2209–2214.

Hongfei Wu (S'11–M'13) was born in Hebei, China, in 1985. He received the B.S. and Ph. D degrees in electrical engineering and power electronics and power drives from Nanjing University of Aeronautics and Astronautics (NUAA), Nanjing, China, in 2008 and 2013, respectively. From June 2012 to July 2012, he was a guest Ph.D. student in the Institute of Energy Technology, Aalborg University, Aalborg, Denmark.

Since 2013, he has been with the Faculty of Electrical Engineering, NUAA, and is currently an Associate Professor with College of Automation Engineering, NUAA. He has authored and co-authored more than 100 peer-reviewed papers published in journals and conference proceedings. He is the holder of more than 20 Patents. His research interests are power converters, distributed power generation and spacecraft power system.

Dr. Wu received the Outstanding Reviewer of IEEE TRANSACTIONS ON POWER ELECTRONICS in 2013.

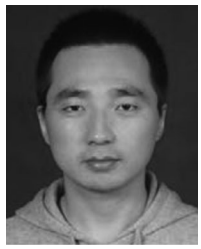

Xiaohai Zhan was born in Hubei, China, in 1990.He received the B.S. degrees in electrical engineering and power electronics and power drives from Nanjing University of Aeronautics and Astronautics (NUAA), Nanjing, China, in 2014. He is currently working toward the M.S. degree in electrical engineering from NUAA.

His research interests include topology and control of soft-switching dc-dc converters.

Yan Xing (M'03) was born in Shandong, China, in 1964. She received the B.S. and M.S. degrees in automation and electrical engineering from Tsinghua University, Beijing, China, in 1985 and 1988, respectively, and the Ph.D. degree in electrical engineering from Nanjing University of Aeronautics and Astronautics (NUAA), Nanjing, China, in 2000.

Since 1988, she has been with the Faculty of Electrical Engineering, NUAA, and is currently a Professor with College of Automation Engineering, NUAA. She has authored more than 100 technical papers published in journals and conference proceedings and has also published three books. Her research interests include topology and control for dc-dc and dc-ac converters.

Dr. Xing is an Associate Editor of the IEEE TRANSACTIONS ON POWER ELECTRONICS and *Journal of Power Electronics*. She is a Member of the Committee on Renewable Energy Systems within the IEEE Industrial Electronics Society.